ISSN 0915-633X

NATIONAL INSTITUTE FOR FUSION SCIENCE

Production Mechanism of Negative Pionlike Particles in H_2 Gas Discharge Plasma

J. Uramoto

(Received - Feb. 21, 1996)

NIFS-414 Apr. 1996

RESEARCH REPORT
NIFS Series

NAGOYA, JAPAN

Production Mechanism of Negative Pionlike Particles in H_2 Gas Discharge Plasma

Jōshin URAMOTO

National Institute for Fusion Science,

Nagoya 464-01, Japan

Abstract

Negative pionlike and muonlike particles are produced by an electron bunch and a positive ion bunch which are generated controllably from an electron beam and a gas. Physical characteristics of the negative pionlike particles are the same with those of negative pionlike particles extracted from the H_2 gas discharge. Thus, the production mechanism in the H_2 gas discharge is deduced.

Keywords: negative pionlike particle, electron bunch,

ion bunch, H_2 gas discharge plasma

1. Introduction

It has been reported already[1] that negative pionlike (π^-) particles are extracted from the outside region of the H_2 gas discharge plasma in magnetic fields, and that a special detection method[2] for the π^- particles is necessary. However, the production mechanism of the π^- particles in the outside region of the plasma has not been clarified.

On the other hand, negative pionlike (π^-) particles or negative muonlike (μ^-) particles have been produced under a different production method[3] using an electron beam and a positive ion beam which are generated controllably. There, the electron beam is bunched magnetically and the positive ion beam is bunched electrically.

Thus, a comparison between the two production methods becomes important to research the production mechanism of the π^- or μ^- particles.

In this paper, the production method by the electron beam and the positive ion beam is reexamined in relation with the detection method[2] of π^- particles extracted from the H_2 gas discharge plasma. Afterward, we will deduce the production mechanism of the π^- particles in the H_2 gas discharge plasma.

2. Reexamination

Schematic diagrams of the experimental apparatus[3] are shown in Fig. 1 and Fig. 2. The first electron beam (F.E.B.) is stopped critically in front of the entrance slit S by an electrical potential of the decelerator D connected to the cathode of the electron gun. Next, a neutral gas is introduced into the first electron beam region and a plasma is produced through ionization of the gas. Then, positive ions of the plasma are accelerated in front of S, while a positive ion beam with an energy corresponding to the first electron beam acceleration voltage V_A is injected into the magnetic field region through S. Moreover, the stopped beam electrons are reaccelerated electrically toward the gap between two magnetic poles (N) and (S) through S, while the injected ion beam is decelerated electrically and stopped in the gap. The electrically reaccelerated electrons are injected perpendicularly to the magnetic field (B_M) and bunched in cyclotron motions of small radius.

As shown in Fig. 2, the above magnetic system is used as a mass analyzer (M.A.) of 90° type when the beam collector B.C. is arranged. The analyzing curvature radius r is 4.3 cm. It

should be noted that the bias voltage V_S of the beam collector is positive with respect to the mass analyzer, and that the back space of the beam collector B.C. is surrounded by an insulator Ins. to interrupt the diffusion of positive ions from the secondary plasma S.P.. This detection method of pionlike particles has reported already for the H_2 gas discharge plasma[2].

A fringe magnetic field distribution of the analyzing magnetic field B_M under a magnetic coil current of 1A, is shown in Fig. 3 for two different metal plates as the entrance plate (decelerator D) of Fig. 1 and Fig. 2. In this experiment, the iron (Fe) plate is used and the fringe magnetic field is much reduced.

The distribution of electrically applied potential are shown in Fig. 4. The first electron beam from the electron gun is perfectly reflected in front of the entrance slit S of the magnetic mass analyzer (M.A.) while a plasma is produced by a gas (air) ionization. Then, a positive ion beam is injected into M.A. through the slit S and the second electron beam is produced by reacceleration of the plasma electrons. It should be noted that the injected positive ion beam (i_2) is decelerated and stopped electrically, and that the second electron beam (e_2) suffers a magnetron (cyclotron) motion in the uniform magnetic field (which is used as the analyzing magnetic field of M.A.). As a result, both the electron beam and positive ion beam will be bunched within the small space at the entrance X of the uniform magnetic field.

Thus, we can expect a coherent interaction between the bunched electrons and positive ions.

For the first experiment of Fig. 2, dependences of a negative current I^- to the beam collector B.C. on the analyzing magnetic field B_M are shown in Fig. 5 for a first electron beam acceleration voltage V_A of 400V under two positive bias voltage V_S of the beam collector V_S = 50V and V_S = 100V. Here, we find that an analyzing relation of the negative muon μ^- is satisfied for the first peak of negative current I^-, if we assume that the effective acceleration voltage V_E is twice of the first electron beam acceleration voltage V_A. That is, the following relation is found: From the analyzing magnetic field B_M where the negative current shows a peak, the curvature radius r of the mass analyzer and the effective acceleration voltage V_E, we can estimate the mass m of the negatively charge particle by,

$$m = \frac{Ze\,(B_M r)^2}{2V_E}$$

$$= \frac{8.8 \times 10^{-2}\, Z\,(B_M r)^2\, m_e}{V_E}, \quad \text{..... (1)}$$

where e is the electron charge, B_M is in gauss unit, r is in cm unit, V_E is in volt unit and m_e is the electron mass and Z is the charge number. For the curvature radius $r = 4.3$ cm of this mass analyzer, the Eq. (1) is rewritten by

$$m = \frac{1.63\, Z\, B_M^2}{V_E} m_e. \quad \text{..... (2)}$$

From Eq. (2) and the experimental conditions for the first peak of I^- of Fig. 5, we obtain $m = m_1 \approx 200\, m_e$ under $V_E = 2V_A = 800$V and $B_M \approx 305$ gauss, assuming that $Z = 1$. This experimental result means that negative muonlike particles μ^- are produced (because the typical muon mass is near 207 m_e).

Moreover, we find the second peak of I^- in Fig. 5. From Eq. (2) and the experimental conditions, we obtain $m = m_2 \approx 285\, m_e$ under $V_E = 800$V and $B_M \approx 370$ gauss. This mass m_2 is near the typical pion mass (273 m_e). That is, negative pionlike particles π^- are produced also.

In the second experiment, the beam collector is interrupted partially by a metal plate MP as shown in Fig. 6. Then, dependences of negative current I^- to the beam collector B.C. on B_M are shown in Fig. 7 for $V_A = 400$V under $V_S = 50$V and $V_S = 100$V. We find that a large part of each negative current peak corresponding to the μ^- or π^- particles appears clearly also. In the first experimental of Fig. 2 or this second experiment of Fig. 6, a positive ion current of about 0.02 μA (for 0.5 cm^2) to the beam collector B.C. is observed when a deep negative bias voltage ($V_S = -350$V) is given to the beam collector. Therefore, we can consider two phenomena for this second experiment: First, the μ^- and π^- particles (or electrons from S.P. in Fig. 6) diffuse around the metal plate MP as ambipolar diffusions due to the positive ions. Second, a large part of the μ^- and π^- particles penetrate the metal plate MP if the positive ions exist behind the metal plate MP.

In order to distinguish two above considerations, the third experiment is tried where the positive ions diffuse to the back space of the beam collector as shown in Fig. 8. Then, as shown in Fig. 9, their negative current peaks of I^- corresponding to the μ^- and π^- particles are much

reduced below 1/20 for the same bias voltage V_S = 100V. If their peaks of Γ^- are due to the ambipolar diffusions, their peak values of Γ^- must increase about twice (in estimation of the opposite side of the beam collector). Thus, we can conclude that a large part of the μ^- or π^- particles penetrate the beam collector B.C. or the metal plate MP[4] if the positive ions diffuse to each back space. On the other hand, the positive ions are not observed in the back space of the beam collector at the first experiment of Fig. 2 while their two peaks of Γ^- appear clearly in larger values of Γ^-.

From the case of V_S = 200V in (3) of Fig. 9, it is obvious that a larger positive bias voltage for the beam collector is necessary in order to suppress the penetration of π^- or μ^- particles.

3. Comparison

Experimental results of the above reexamination are similar to those[1),2)] of the H_2 gas discharge plasma in magnetic fields. Inversely, the production mechanism of the π^- particles in the H_2 gas discharge plasma can be deduced from the above experiments: The schematic diagram of experimental apparatus for the H_2 gas discharge plasma is shown in Fig.10. First, a low energy positive ion beam may be produced by the first extraction electrode (L) whose potential is kept around –15V with respect to the anode (12 in Fig.10). Because the magnetic field (B_Z in Fig.10) B_Z applied along the sheet plasma, is very weak for the positive ions. That is, the positive ion Larmor radius is very large and around 10 cm (as the acceleration voltage of 15V for H_3^+ ion under $B_Z \approx$ 50 gauss). When the low energy positive ion beam enters between the first extraction electrode L and the intermediate electrode M, the ion beam is decelerated by the positive potential (+100V ~ +300V) of M and may be bunched electrically.

Next, the electrons in the H_2 gas discharge plasma are distributed all over the plasma space and the ion beam space charge is compensated while an strong interaction between an electron bunch and an ion bunch does not occur. However, if the low energy components of the (thermal) electrons are much absorbed by the volume production of H^- ions, some high energy components (above 3 eV) of the electrons remain in the ion beam. Then, the electron Larmor radius is around 0.1 cm (as the electron temperature of 3 eV), which is very small in comparison with that of the positive ion.

From these estimations, we may expect a strong space charge interaction between the ion bunch and the high energy electron bunch.

In conclusion, we consider that the two above[1, 3] production mechanisms are the same physically.

References

1) J. Uramoto: National Institute of Fusion Science, Nagoya, Japan-Research Report, NIFS-377 (1995).

2) J. Uramoto: NIFS- 400(1996).

3) J. Uramoto: NIFS-277 (1994).

4) J. Uramoto: NIFS-350 (1995).

Figure Captions

Fig. 1 and Fig. 2: Schematic diagrams of the experimental apparatus.

F: Filament as electron emitter. K: Cathode of electron gun. A: Anode of electron gun. V_A: Initial electron acceleration voltage. I_A: Total negative current. F.E.B.: First electron beam. G: Neutral gas. D: Decelerator of F.E.B. S: Entrance slit (3 mm × 10 mm). Ins: Insulator. I.B.: Ion beam. S.E.B.: Second electron beam. e: Electrons with cyclotron motions. μ^-: Negative muonlike particle. (M.A.): Mass analyzer. Fe: Iron. C: Magnetic Coil. (N): North pole of electro-magnet. (S): South pole. B_M: Analyzing magnetic field. B.C.: Beam collector. Γ^-: Negative current to B.C. V_S: Bias voltage of B.C. with respect to mass analyzer body. S.P.: Secondary plasma inside (M.A.). X: Entrance of uniform magnetic field. i: Ion bunch. π^-: Negative pionlike particle. Ins: Insulator. +Ion: Positive ion.

Fig. 3 Fringe magnetic field distribution (at 1A of magnetic coil current).

B_M: Analyzing magnetic field of (M.A.). B_O: Uniform magnetic field inside (M.A.). X: End of uniform magnetic field. S: Entrance slit position. Fe: Magnetic field distribution in a case using iron plate as D in Fig. 1. Cu: Magnetic field distribution in a case using copper plate as D in Fig. 1.

Fig. 4 Applied electrical potential distribution

V: Electrical potential. V_A: Initial potential (voltage) of electron gun anode. V_E: Effective potential for μ^- (negative muonlike particle) and π^- (negative pionlike particle). e_0: Initial electrons from electron gun cathode. e_1: First electron beam. e_2: Second electron beam. i_1: Positive ion beam from plasma. i_2: Second positive ion beam. e–B: Electron bunch due to magnetic cyclotron motion. i–B: Positive ion bunch due to electrical retardation. K: Cathode position of electron gun. A: Anode position of electron gun. S: Slit position of mass analyzer. X: Entrance position of analyzing uniform magnetic field. $+V_A$: Additional potential generated by stopping the positive ion beam.

Fig. 5 Dependences of the negative beam collector current I^- on the analyzing magnetic field B_M when the diffusion of positive ions to the back of the beam collector is interrupted as shown in Fig. 2.

(1): Beam collector bias voltage V_S = 50V. (2): V_S = 100V. First electron beam acceleration voltage V_A = 400V. Total anode current I_A = 3.0 mA (see Fig. 1). Gas pressure (air) is 1×10^{-5} Torr (G region in Fig. 1). μ^-: means negative muonlike particle. π^-: means negative pionlike particle. e: means electron current near $B_M \approx 0$.

Fig. 6 A schematic diagram of the experimental apparatus where a metal plate MP is put partially in front of the beam collector.

MP: Copper plate of 0.5 mm in thickness. (see Fig. 1 and Fig. 2 also.)

Fig. 7 Dependences of the negative beam collector current I^- on the analyzing magnetic field B_M corresponding to Fig. 6.

(1): Beam collector bias voltage V_S = 50V. (2): V_S = 100V. First electron beam acceleration voltage V_A = 400V. Total anode current I_A = 3.0 mA (see Fig. 1). Gas pressure (air) is 1×10^{-5} Torr (G region in Fig. 1). μ^-: means negative muonlike particle. π^-: means negative pionlike particle. e: means diffused electrons.

Fig. 8 A schematic diagram where the positive ions diffuse to the back space of the beam collector. +Ion: Positive ion. (see Fig. 1 and Fig. 2 also.)

Fig. 9 Dependences of I^- on B_M corresponding to Fig. 8.

(2): Beam collector bias voltage V_S = 100V. (3): V_S = 200V. First electron beam acceleration voltage V_A = 400V. Total anode current I_A = 3.0 mA (see Fig. 1). Gas pressure (air) is 1×10^{-5} Torr (G region in Fig. 1). μ^-: means negative muonlike particle. π^-: means negative pionlike particle. e: means electrons.

Fig. 10 Schematic diagram of experimental apparatus for H_2 gas discharge.

1: Cylindrical plasma in discharge anode. 2: Discharge cathode. 3: H_2 gas flow. 4: Discharge power supply. 5: Electron acceleration power supply. 6: Vacuum pump. 7: Area where cylindrical plasma is transformed into sheet plasma. 8: Insulation tube. 9: A pair of permanent magnets. 10: Magnetic field coils. 11: Slit of acceleration anode. 12: Electron acceleration anode. 13: Floated end electrode. I_A: Current to electron acceleration anode. CP: Cylindrical plasma. SP: Sheet plasma. B_Z: Magnetic field. L: First extraction electrode. M: Second extraction electrode. E: Final extraction electrode. V_M: Potential of second extraction electrode with respect to electron acceleration anode. V_E: Potential of final extraction electrode with respect to electron acceleration anode. I_E: Negative current to final extraction electrode. MA: Magnetic deflection (90°) mass analyzer. B_M: Magnetic field intensity of MA. BC: Beam collector of MA. V_{BC}: Positive potential of BC with respect to MA. I^-: Negative current to BC. I_{MA}: Total negative current to MA. H_0^-: Hydrogen negative ions outside of sheet plasma. H^-: Accelerated hydrogen negative ions. π_0^-: Negative pionlike particles outside of sheet plasma. π^-: Accelerated negative pionlike particles.

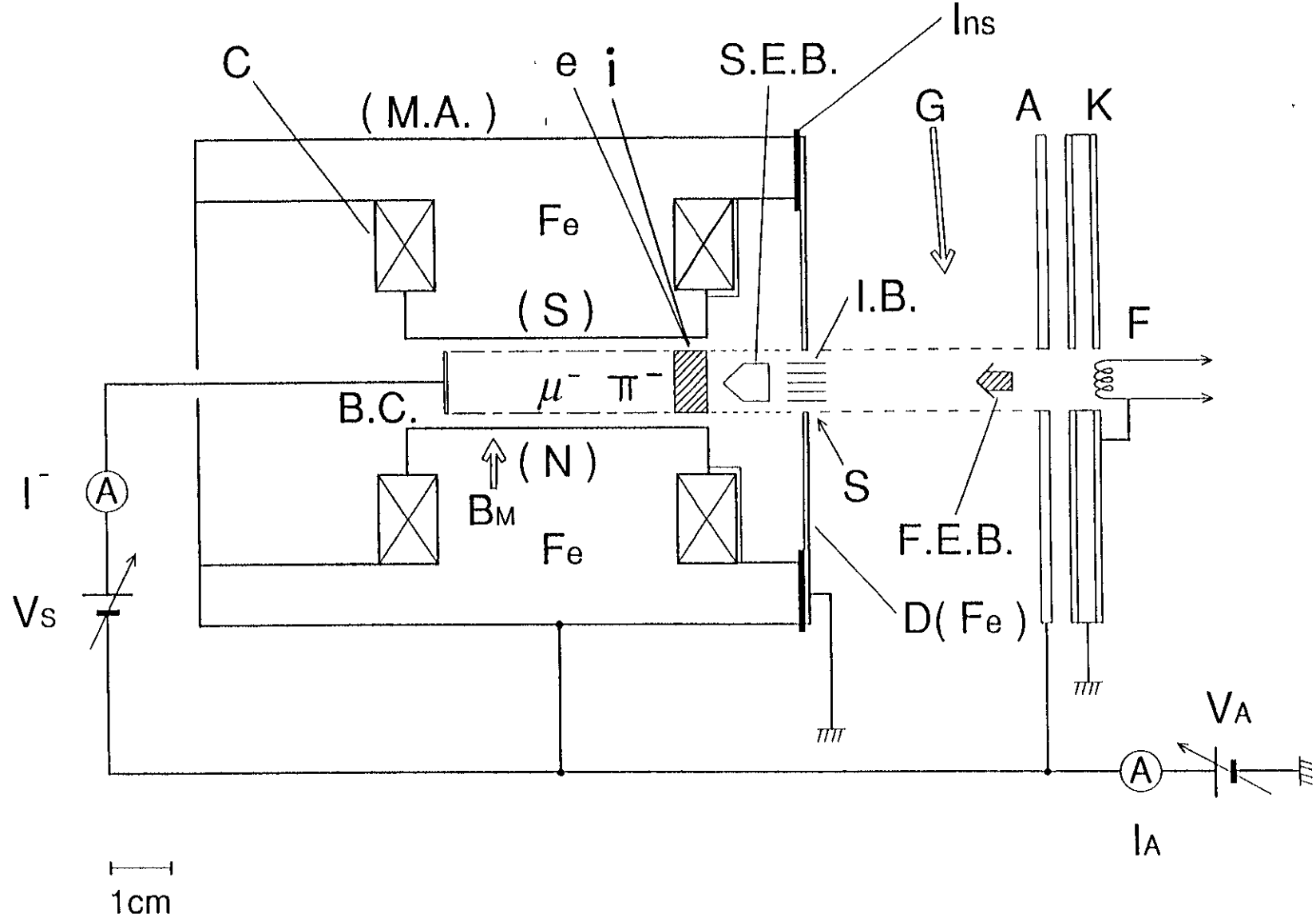

Fig. 1

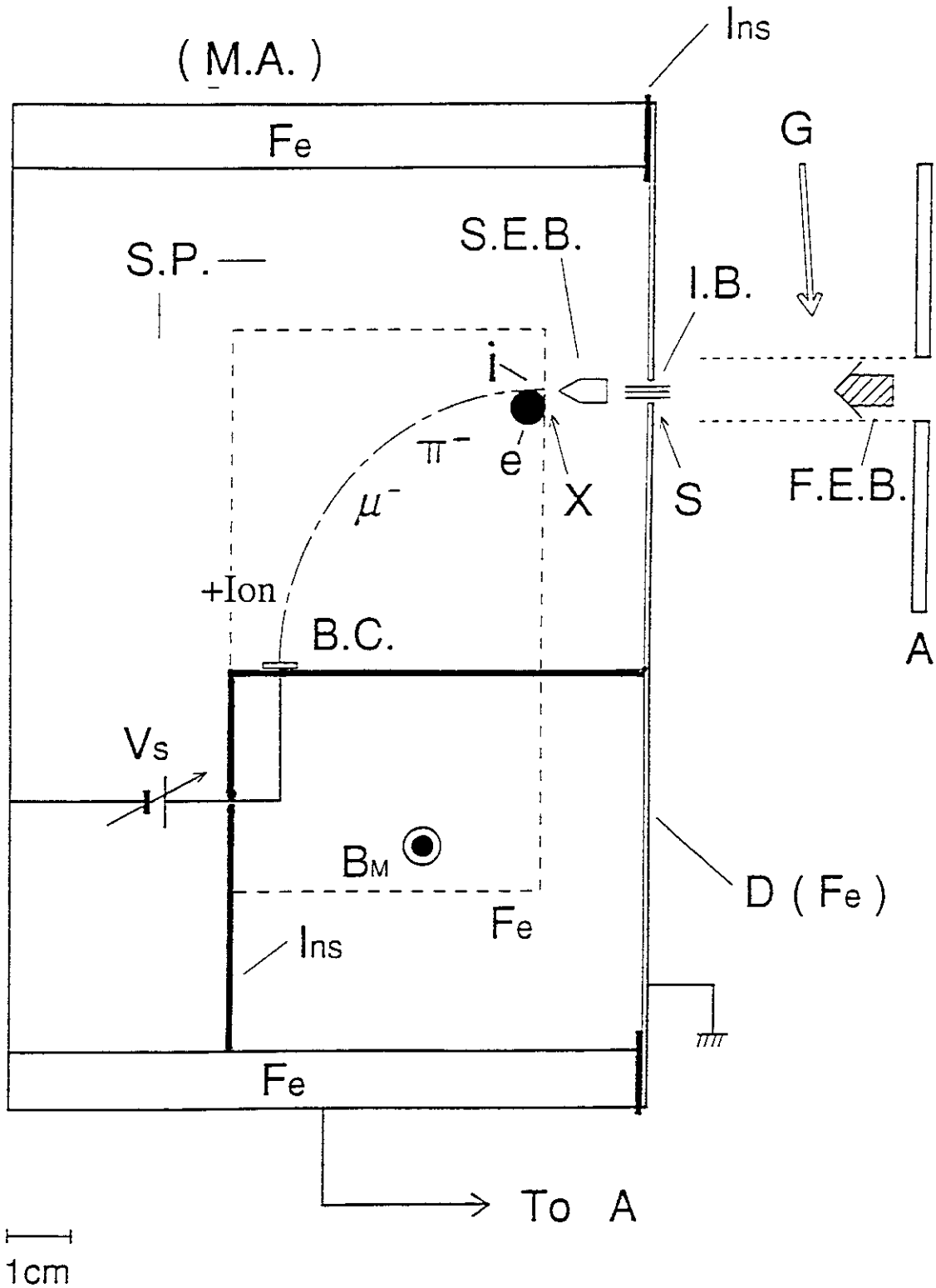
(M.A.)
Ins
Fe
G
S.P.
S.E.B.
I.B.
i
π⁻
e
μ⁻
X
S
F.E.B.
+Ion
B.C.
A
Vs
BM
D (Fe)
Fe
Ins
Fe
To A
1cm

Fig. 2

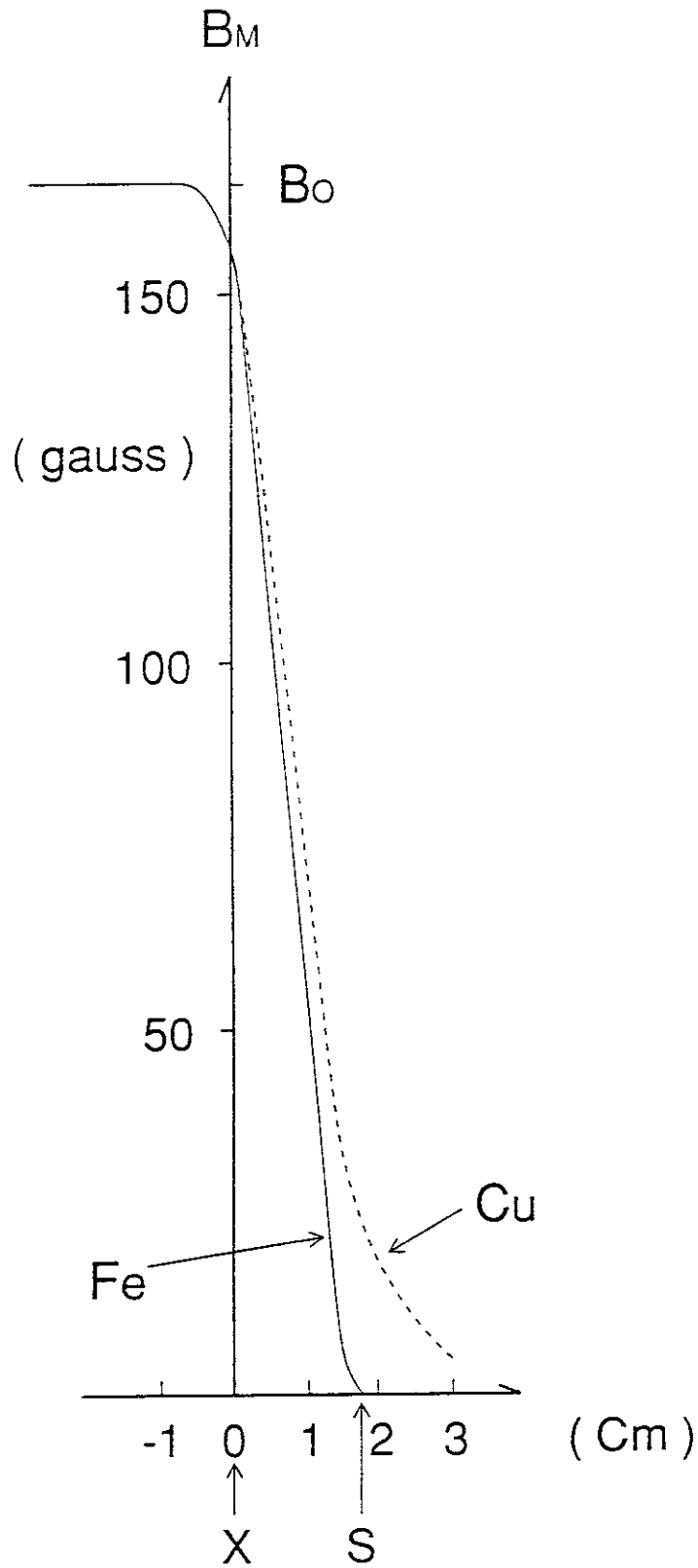

Fig. 3

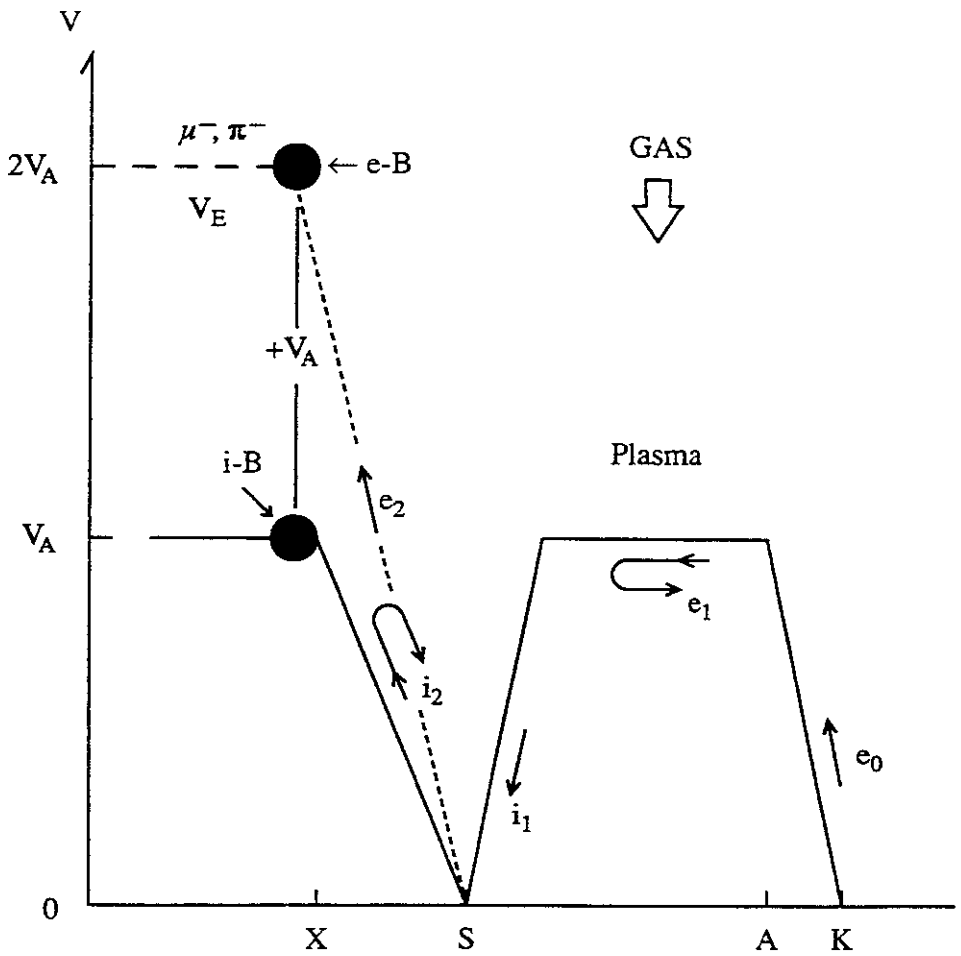

Fig. 4

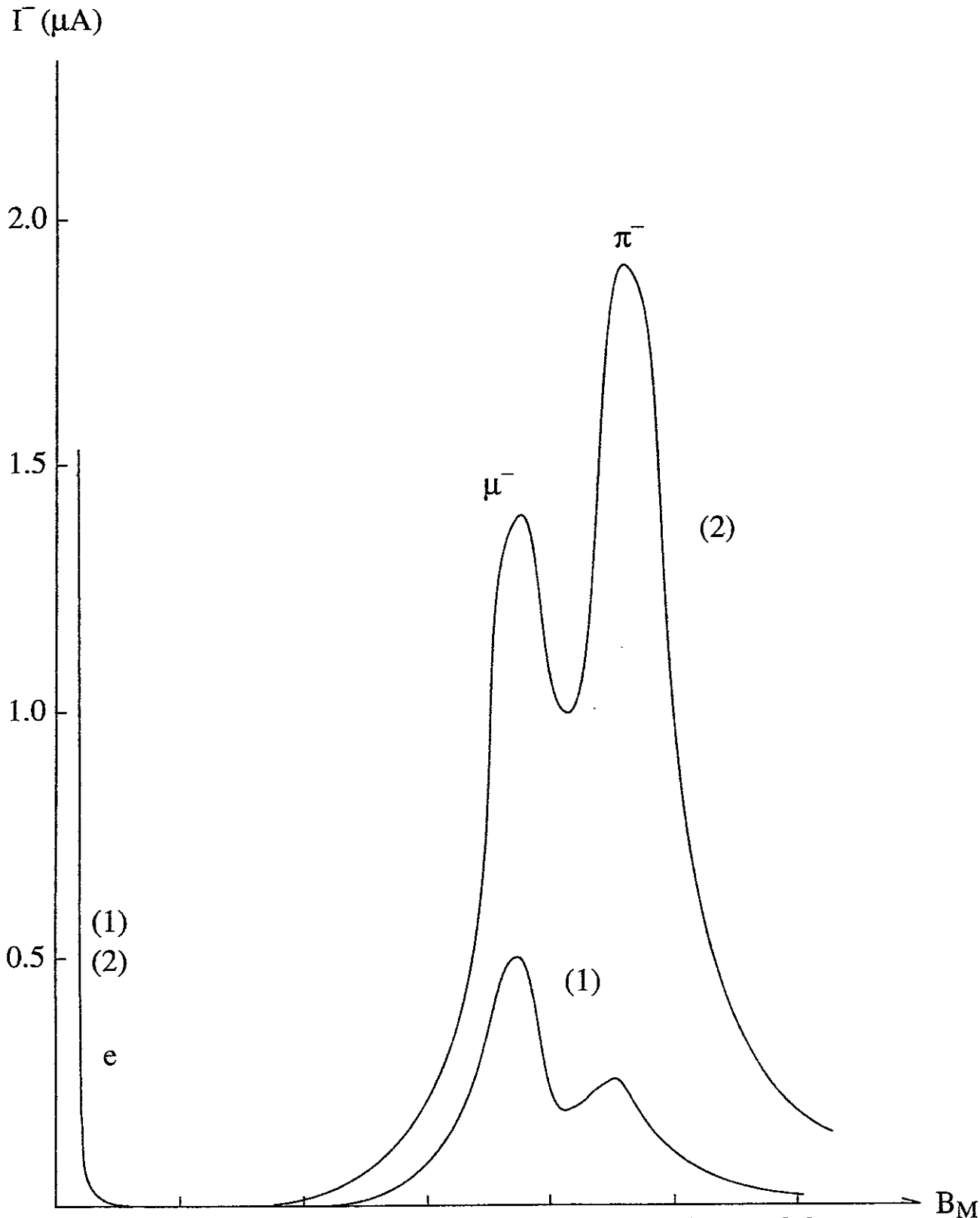

Fig. 5

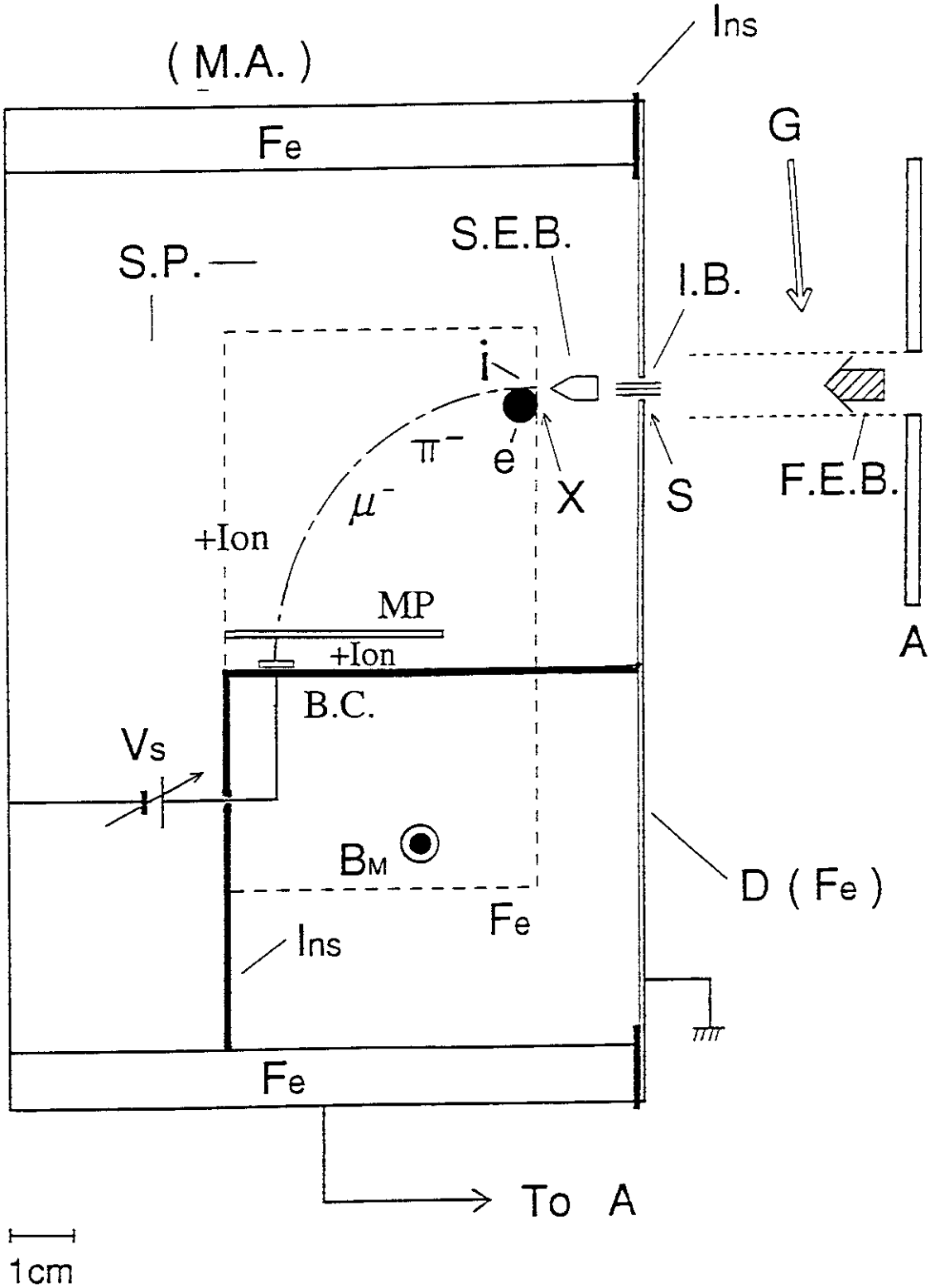
(M.A.)
Ins
Fe
G
S.E.B.
S.P.
I.B.
i
π⁻
e
μ⁻
X
S
F.E.B.
+Ion
MP
+Ion
A
B.C.
Vs
BM
D (Fe)
Fe
Ins
Fe
To A
1cm

Fig. 6

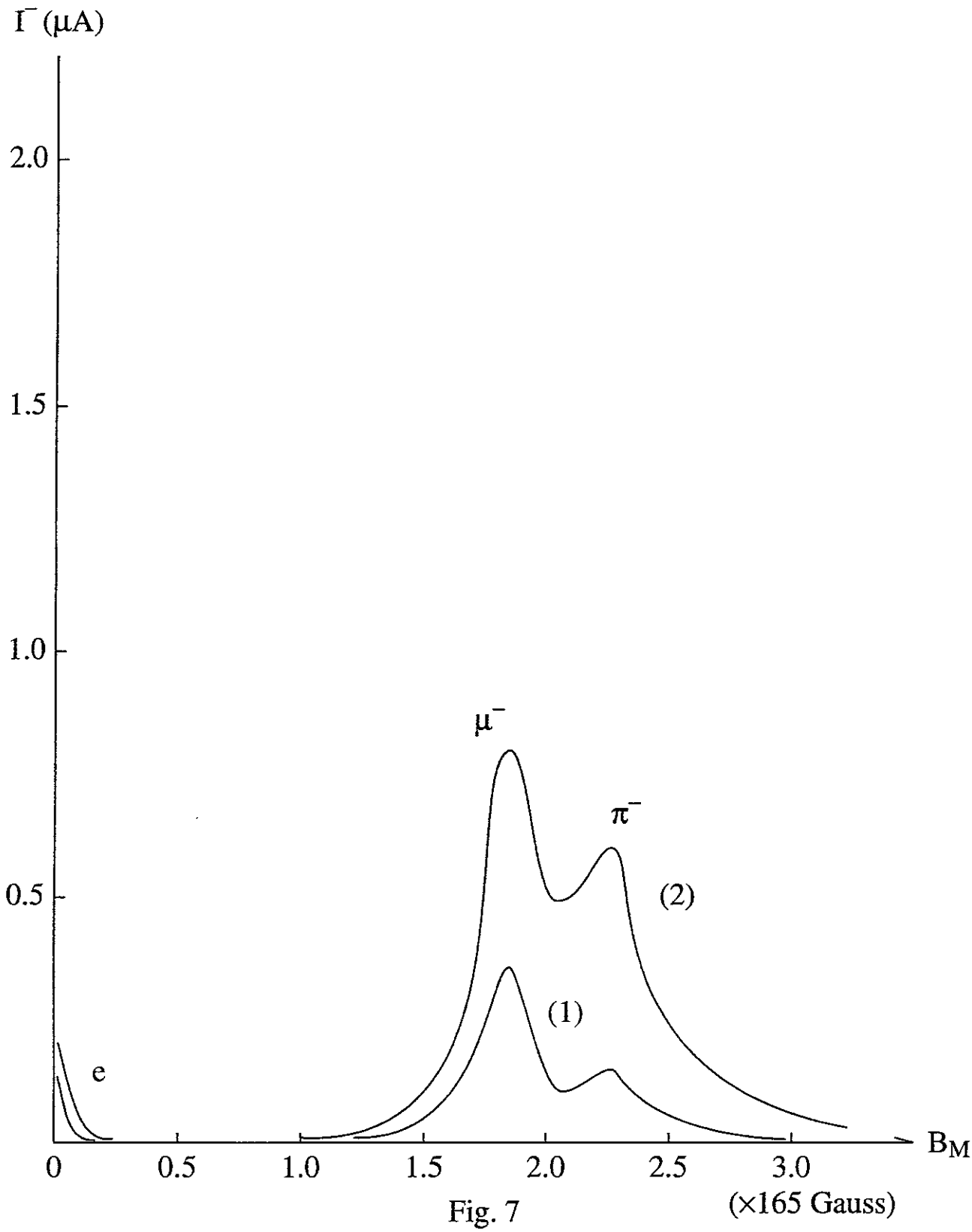

Fig. 7

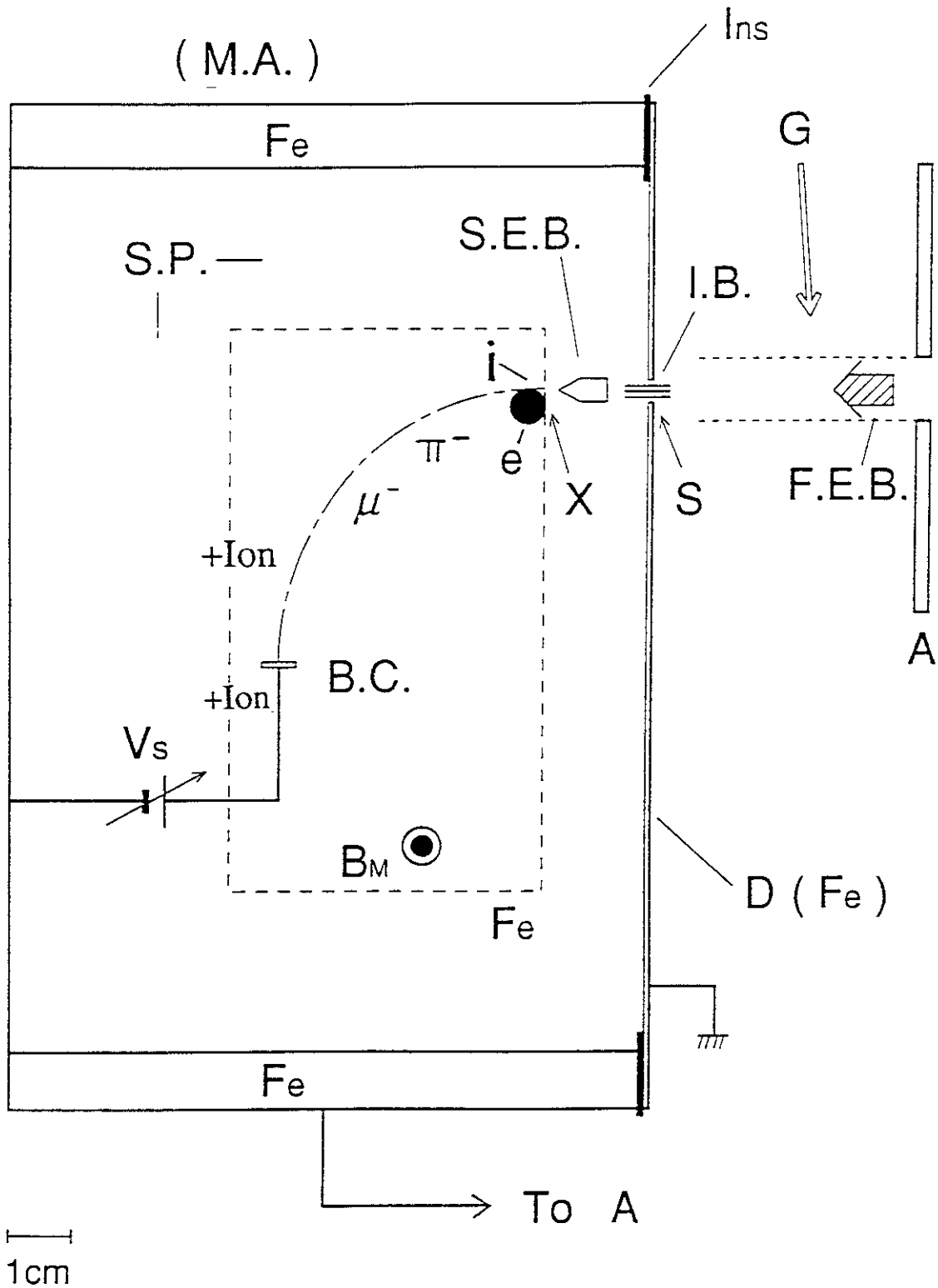
(M.A.)
Ins
Fe
G
S.P.
S.E.B.
I.B.
i
π⁻
e
μ⁻
X
S
F.E.B.
+Ion
A
B.C.
+Ion
Vs
BM
D (Fe)
Fe
Fe
To A
1cm

Fig. 8

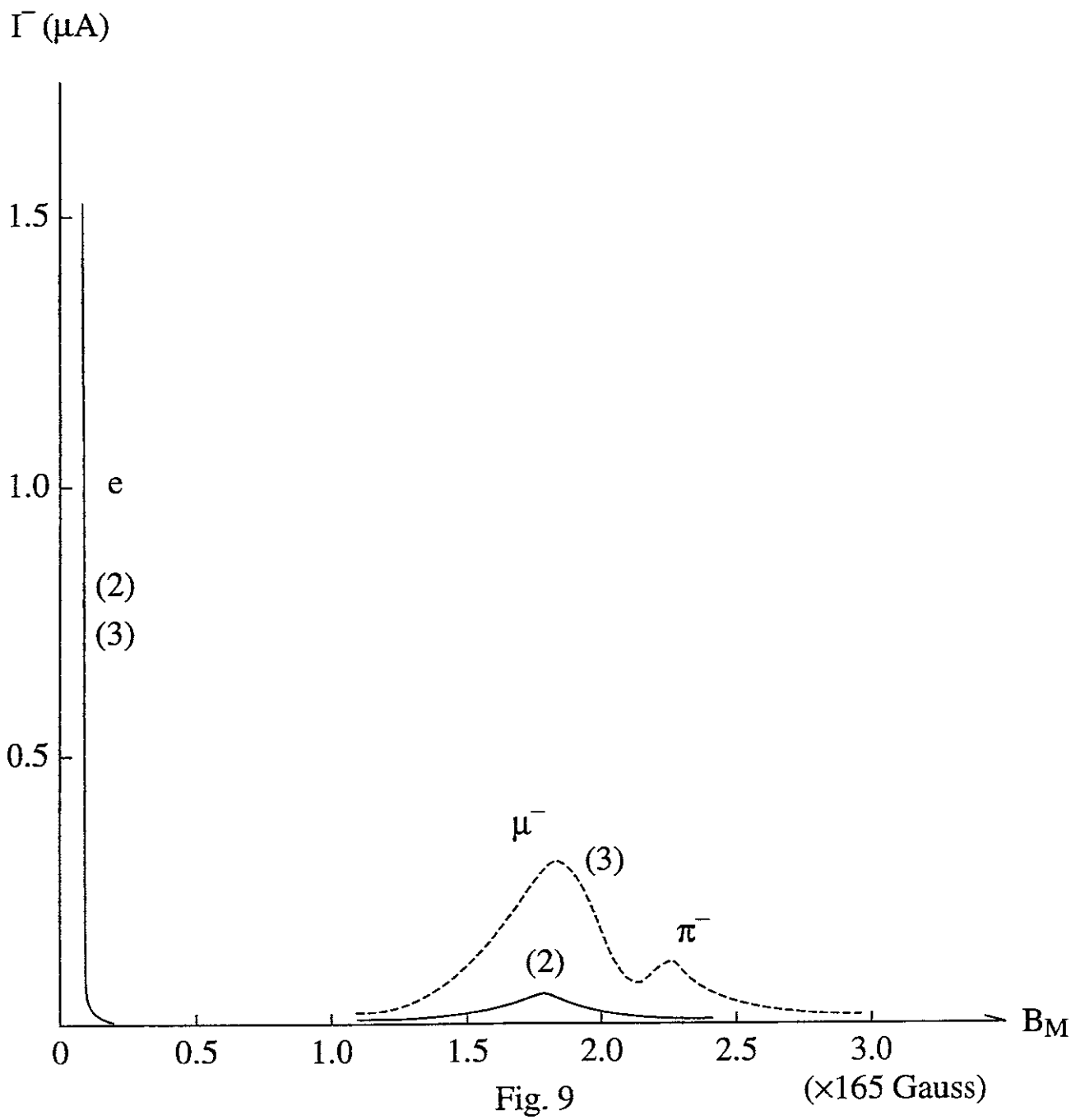

Fig. 9

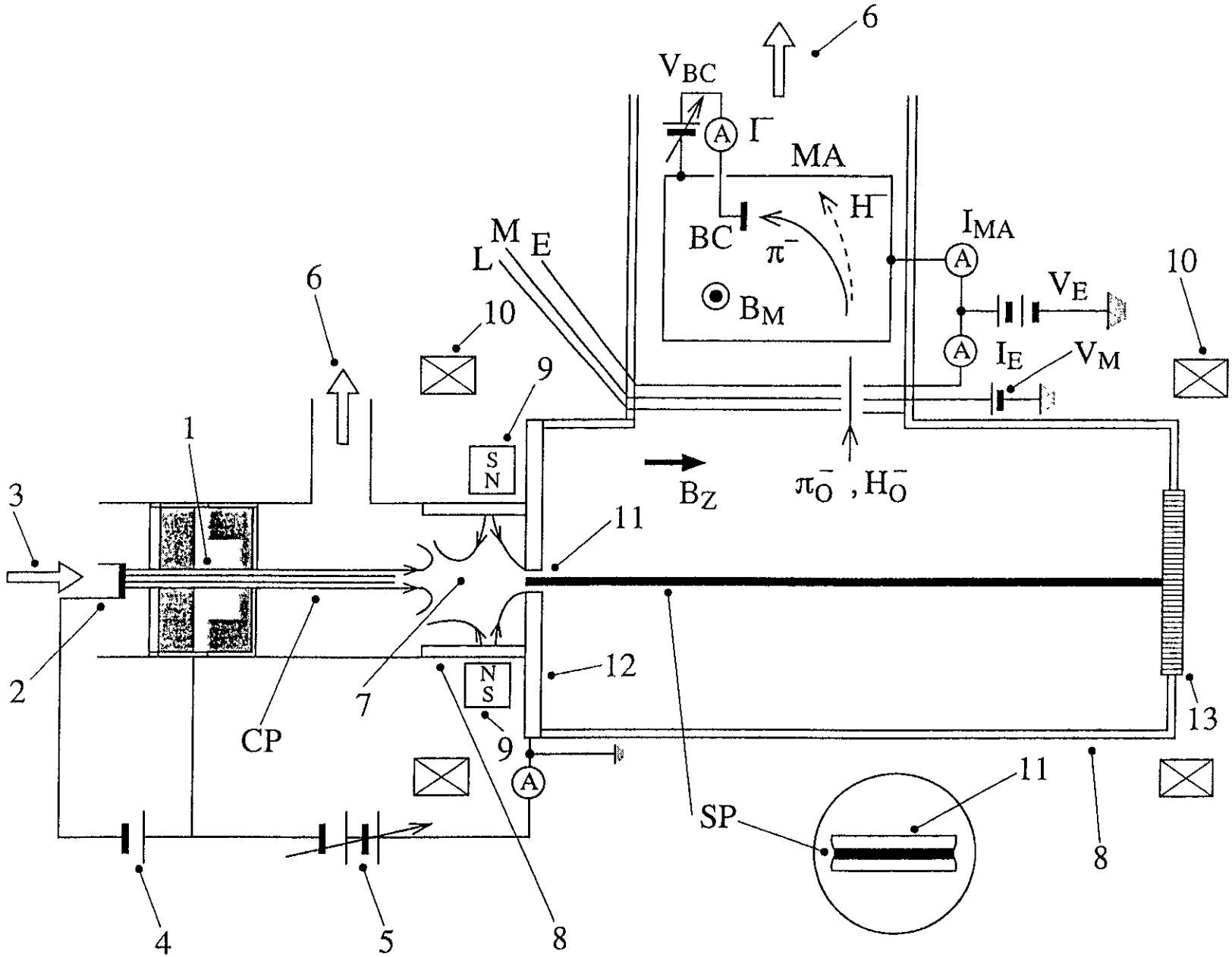
6
V_{BC}
A
Γ
MA
H⁻
BC
π⁻
B_M
M
L
E
I_{MA}
A
V_E
A
I_E
V_M
10
10
6
9
1
S
N
B_Z
π_O^- , H_O^-
3
11
2
CP
7
N
S
12
13
9
A
11
SP
8
4
5
8

Fig. 10

Recent Issues of NIFS Series

NIFS-366 K. Itoh and Sanae-I. Itoh,
The Role of Electric Field in Confinement; July 1995

NIFS-367 F. Xiao and T. Yabe,
A Rational Function Based Scheme for Solving Advection Equation; July 1995

NIFS-368 Y. Takeiri, O. Kaneko, Y. Oka, K. Tsumori, E. Asano, R. Akiyama, T. Kawamoto and T. Kuroda,
Multi-Beamlet Focusing of Intense Negative Ion Beams by Aperture Displacement Technique; Aug. 1995

NIFS-369 A. Ando, Y. Takeiri, O. Kaneko, Y. Oka, K. Tsumori, E. Asano, T. Kawamoto, R. Akiyama and T. Kuroda,
Experiments of an Intense H- Ion Beam Acceleration; Aug. 1995

NIFS-370 M. Sasao, A. Taniike, I. Nomura, M. Wada, H. Yamaoka and M. Sato,
Development of Diagnostic Beams for Alpha Particle Measurement on ITER; Aug. 1995

NIFS-371 S. Yamaguchi, J. Yamamoto and O. Motojima;
A New Cable -in conduit Conductor Magnet with Insulated Strands; Sep. 1995

NIFS-372 H. Miura,
Enstrophy Generation in a Shock-Dominated Turbulence; Sep. 1995

NIFS-373 M. Natsir, A. Sagara, K. Tsuzuki, B. Tsuchiya, Y. Hasegawa, O. Motojima,
Control of Discharge Conditions to Reduce Hydrogen Content in Low Z Films Produced with DC Glow; Sep. 1995

NIFS-374 K. Tsuzuki, M. Natsir, N. Inoue, A. Sagara, N. Noda, O. Motojima, T. Mochizuki, I. Fujita, T. Hino and T. Yamashina,
Behavior of Hydrogen Atoms in Boron Films during H_2 and He Glow Discharge and Thermal Desorption; Sep. 1995

NIFS-375 U. Stroth, M. Murakami, R.A. Dory, H. Yamada, S. Okamura, F. Sano and T. Obiki,
Energy Confinement Scaling from the International Stellarator Database; Sep. 1995

NIFS-376 S. Bazdenkov, T. Sato, K. Watanabe and The Complexity Simulation Group,
Multi-Scale Semi-Ideal Magnetohydrodynamics of a Tokamak Plasma; Sep. 1995

NIFS-377 J. Uramoto,

Extraction of Negative Pionlike Particles from a H2 or D2 Gas Discharge Plasma in Magnetic Field; Sep. 1995

NIFS-378 K. Akaishi,
Theoretical Consideration for the Outgassing Characteristics of an Unbaked Vacuum System; Oct. 1995

NIFS-379 H. Shimazu, S. Machida and M. Tanaka,
Macro-Particle Simulation of Collisionless Parallel Shocks; Oct. 1995

NIFS-380 N. Kondo and Y. Kondoh,
Eigenfunction Spectrum Analysis for Self-organization in Dissipative Solitons; Oct. 1995

NIFS-381 Y. Kondoh, M. Yoshizawa, A. Nakano and T. Yabe,
Self-organization of Two-dimensional Incompressible Viscous Flow in a Friction-free Box; Oct. 1995

NIFS-382 Y.N. Nejoh and H. Sanuki,
The Effects of the Beam and Ion Temperatures on Ion-Acoustic Waves in an Electron Beam-Plasma System; Oct. 1995

NIFS-383 K. Ichiguchi, O. Motojima, K. Yamazaki, N. Nakajima and M. Okamoto
Flexibility of LHD Configuration with Multi-Layer Helical Coils; Nov. 1995

NIFS-384 D. Biskamp, E. Schwarz and J.F. Drake,
Two-dimensional Electron Magnetohydrodynamic Turbulence; Nov. 1995

NIFS-385 H. Kitabata, T. Hayashi, T. Sato and Complexity Simulation Group,
Impulsive Nature in Collisional Driven Reconnection; Nov. 1995

NIFS-386 Y. Katoh, T. Muroga, A. Kohyama, R.E. Stoller, C. Namba and O. Motojima,
Rate Theory Modeling of Defect Evolution under Cascade Damage Conditions:The Influence of Vacancy-type Cascade Remnants and Application to the Defect Production Chracterization by Microstructural Analysis; Nov. 1995

NIFS-387 K. Araki, S. Yanase and J. Mizushima,
Symmetry Breaking by Differential Rotation and Saddle-node Bifurcation of the Thermal Convection in a Spherical Shell; Dec. 1995

NIFS-388 V.D. Pustovitov,
Control of Pfirsch-Schlüter Current by External Poloidal Magnetic Field in Conventional Stellarators: Dec. 1995

NIFS-389 K. Akaishi,
On the Outgassing Rate Versus Time Characteristics in the Pump-down of

an Unbaked Vacuum System; Dec. 1995

NIFS-390 K.N. Sato, S. Murakami, N. Nakajima, K. Itoh,
Possibility of Simulation Experiments for Fast Particle Physics in Large Helical Device (LHD); Dec. 1995

NIFS-391 W.X.Wang, M. Okamoto, N. Nakajima, S. Murakami and N. Ohyabu,
A Monte Carlo Simulation Model for the Steady-State Plasma in the Scrape-off Layer; Dec. 1995

NIFS-392 Shao-ping Zhu, R. Horiuchi, T. Sato and The Complexity Simulation Group,
Self-organization Process of a Magnetohydrodynamic Plasma in the Presence of Thermal Conduction; Dec. 1995

NIFS-393 M. Ozaki, T. Sato, R. Horiuchi and the Complexity Simulation Group
Electromagnetic Instability and Anomalous Resistivity in a Magnetic Neutral Sheet; Dec. 1995

NIFS-394 K. Itoh, S.-I Itoh, M. Yagi and A. Fukuyama,
Subcritical Excitation of Plasma Turbulence; Jan. 1996

NIFS-395 H. Sugama and M. Okamoto, W. Horton and M. Wakatani,
Transport Processes and Entropy Production in Toroidal Plasmas with Gyrokinetic Eletromagnetic Turbulence; Jan. 1996

NIFS-396 T. Kato, T. Fujiwara and Y. Hanaoka,
X-ray Spectral Analysis of Yohkoh BCS Data on Sep. 6 1992 Flares - Blue Shift Component and Ion Abundances -; Feb. 1996

NIFS-397 H. Kuramoto, N. Hiraki, S. Moriyama, K. Toi, K. Sato, K. Narihara, A. Ejiri, T. Seki and JIPP T-IIU Group,
Measurement of the Poloidal Magnetic Field Profile with High Time Resolution Zeeman Polarimeter in the JIPP T-IIU Tokamak; Feb. 1996

NIFS-398 J.F. Wang, T. Amano, Y. Ogawa, N. Inoue,
Simulation of Burning Plasma Dynamics in ITER; Feb. 1996

NIFS-399 K. Itoh, S-I. Itoh, A. Fukuyama and M. Yagi,
Theory of Self-Sustained Turbulence in Confined Plasmas; Feb. 1996

NIFS-400 J. Uramoto,
A Detection Method of Negative Pionlike Particles from a H2 Gas Descharge Plasma; Feb. 1996

NIFS-401 K.Ida, J.Xu, K.N.Sato, H.Sakakita and JIPP TII-U group,
Fast Charge Exchange Spectroscopy Using a Fabry-Perot Spectrometer in the JIPP TII-U Tokamak; Feb. 1996

NIFS-402 T. Amano,

Passive Shut-Down of ITER Plasma by Be Evaporation; Feb. 1996

NIFS-403 K. Orito,
A New Variable Transformation Technique for the Nonlinear Drift Vortex; Feb. 1996

NIFS-404 T. Oike, K. Kitachi, S. Ohdachi, K. Toi, S. Sakakibara, S. Morita, T. Morisaki, H. Suzuki, S. Okamura, K. Matsuoka and CHS group;
Measurement of Magnetic Field Fluctuations near Plasma Edge with Movable Magnetic Probe Array in the CHS Heliotron/Torsatron; Mar. 1996

NIFS-405 S.K. Guharay, K. Tsumori, M. Hamabe, Y. Takeiri, O. Kaneko, T. Kuroda,
Simple Emittance Measurement of H- Beams from a Large Plasma Source; Mar. 1996

NIFS-406 M. Tanaka and D. Biskamp,
Symmetry-Breaking due to Parallel Electron Motion and Resultant Scaling in Collisionless Magnetic Reconnection; Mar. 1996

NIFS-407 K. Kitachi, T. Oike, S. Ohdachi, K. Toi, R. Akiyama, A. Ejiri, Y. Hamada, H.Kuramoto, K. Narihara, T. Seki and JIPP T-IIU Group,
Measurement of Magnetic Field Fluctuations within Last Closed Flux Surface with Movable Magnetic Probe Array in the JIPP T-IIU Tokamak; Mar. 1996

NIFS-408 K. Hirose, S. Saito and Yoshi.H. Ichikawa
Structure of Period-2 Step-1 Accelerator Island in Area Preserving Maps; Mar. 1996

NIFS-409 G.Y.Yu, M. Okamoto, H. Sanuki, T. Amano,
Effect of Plasma Inertia on Vertical Displacement Instability in Tokamaks; Mar. 1996

NIFS-410 T. Yamagishi,
Solution of Initial Value Problem of Gyro-Kinetic Equation; Mar. 1996

NIFS-411 K. Ida and N. Nakajima,
Comparison of Parallel Viscosity with Neoclassical Theory; Apr. 1996

NIFS-412 T. Ohkawa and H. Ohkawa,
Cuspher, A Combined Confinement System; Apr. 1996

NIFS-413 Y. Nomura, Y.H. Ichikawa and A.T. Filippov,
Stochasticity in the Josephson Map; Apr. 1996

NIFS-414 J. Uramoto,
Production Mechanism of Negative Pionlike Particles in H_2 Gas Discharge Plasma; Apr. 1996